Hindawi
Journal of Analytical Methods in Chemistry
Volume 2021, Article ID 6613154, 7 pages
https://doi.org/10.1155/2021/6613154

Research Article

Fabrication of SiO_2/PEGDA Inverse Opal Photonic Crystal with Fluorescence Enhancement Effects

Van-Phuc Dinh,[1,2] **Duy-Khoi Nguyen**,[1,2] **Quang-Hung Nguyen**,[2,3] **Thi-Thuy Luu**,[1,2] **Thi Hai Yen Pham**,[4] **Thi Thu Ha Vu**,[4] **Han-Sheng Chuang**,[5] **and Hong-Phong Pham**[4,6]

[1]*Future Materials & Devices Laboratory, Institute of Fundamental and Applied Sciences, Duy Tan University, Ho Chi Minh City 700000, Vietnam*
[2]*Faculty of Environmental and Chemical Engineering, Duy Tan University, Da Nang 550000, Vietnam*
[3]*Institute of Fundamental and Applied Sciences, Duy Tan University, Ho Chi Minh City 700000, Vietnam*
[4]*Institute of Chemistry, Vietnam Academy of Science and Technology, 18-Hoang Quoc Viet Road, Cau Giay, Ha Noi, Vietnam*
[5]*Department of Biomedical Engineering, National Cheng Kung University, Tainan 701, Taiwan*
[6]*Graduate University of Science and Technology, 18- Hoang Quoc Viet Road, Cau Giay, Ha Noi, Vietnam*

Correspondence should be addressed to Hong-Phong Pham; phphong@ich.vast.vn

Received 16 October 2020; Revised 13 January 2021; Accepted 1 February 2021; Published 25 February 2021

Academic Editor: Thi Anh Huong Nguyen

The present paper reports the fabrication of inverse opal photonic crystals (IOPCs) by using SiO_2 spherical particles with a diameter of 300 nm as an opal photonic crystal template and poly(ethylene glycol) diacrylate (PEGDA) as an inverse opal material. Characteristics and fluorescence properties of the fabricated IOPCs were investigated by using the Fourier transform infrared spectroscopy (FTIR), scanning electron microscopy (SEM), X-ray diffraction (XRD), reflection spectroscopy, and fluorescence microscopy. The results clearly showed that the IOPCs were formed comprising of air spheres with a diameter of ~270 nm. The decrease in size led to a decrease in the average refractive indexes from 1.40 to 1.12, and a remarkable stopband blue shift for the IOPCs was thus achieved. In addition, the obtained results also showed a fluorescence enhancement over 7.7-fold for the Fluor® 488 dye infiltrated onto the IOPCs sample in comparison with onto the control sample.

1. Introduction

Photonic crystals (PhC) with a periodic structure have significant effects on the propagation of electromagnetic (EM) waves due to the diffraction of photons in a limited wavelength range from the lattice planes [1, 2], leading to the allowance or restriction of the propagation of EM waves through the material structure. When the EM radiation is forbidden in the wavelength region, it cannot be transmitted, resulting in the reflection from the crystal lattice, known as Bragg diffraction [3]. As the result, the photonic bandgap (PBG) is formed. The changes in the refractive index of PhC lead to the adjustment of the PBG wavelengths and reflection intensity. Consequently, the photonic especially fluorescent properties of the materials are changed [4, 5].

SiO_2 material with a porous structure, known as a stably, nontoxically, harmlessly and low-costly photonic crystalline material, has been widely applied to various areas, such as catalyst supports [6–8], adsorbents [9–11], chromatographic materials [12, 13], and biosensors [14, 15]. In particular, the SiO_2 inverse opal photonic crystal (IOPC) biosensors have been fabricated based on changes in their photoluminescence properties or reflective spectra. It has been shown in the literature [16] that the IOPCs can change not only the wavelengths of PBGs but also enhance the fluorescent intensity. Materials used as the inverse opal materials for fabrication of IOPCs are varieties of hydrogels, such as polystyrene [5, 17], poly(4-vinylbenzyl chloride-co-methyl methacrylate) [18], and poly(styrene-co-methyl methacrylate-co-acrylic acid) [19].

Although poly(ethylene glycol) diacrylate (PEGDA) is a derivative of polyethylene glycol and has been widely used for various biomedical applications due to its biocompatibility [20] and easy excretion from the body [21], the use of this hydrogel as an inverse opal material in IOPCs has still been limited. For instance, studies of Park et al. focused on the fabrication of humidity sensors and biosensors for the detection of immunoglobulin G [22, 23]. Though the obtained results clearly show the change in colour of the fabricated IOPCs with the presence of detection targets, the improvement of fluorescence intensity of IOPCs is still required to enhance the sensitivity of target detections.

In order to fabricate the IOPCs, two techniques have been widely used, namely, thermal degradation [5, 17–19, 24] and chemical etching [25, 26]. The thermal degradation has been commonly used for the treatment of organic templates, while the chemical etching has been regularly applied to remove the inorganic templates, such as TiO_2, ZnO, and SiO_2. Among the chemical etchants, the buffered oxide etch (BOE), a mixture of hydrofluoric acid (HF) and ammonium fluoride (NH_4F), is often used for etching silicon dioxide on the silicon wafers. In this work, SiO_2 spherical particles are used as an opal photonic crystal material, whereas PEGDA is utilized as an inverse opal material to fabricate the IOPCs having two-dimensional periodical and microporous structure with the lattice spacing on the order of the wavelength of light. These IOPCs thus not only induce a stopband shift but also exhibit a fluorescence enhancement for Alexa Fluor® 488 dye, which is a green fluorophore and has been commonly used in applications such as immunolabeling, fluorescence microscopy, and flow cytometry.

2. Materials and Methods

2.1. Chemicals. Nonfunctionalized silica microspheres with a diameter of 300 nm were purchased from the Polyscience Asia Pacific Inc. Poly(ethylene glycol) diacrylate (Mn = 250), ethanol 95%, 2-hydroxy-2-methylpropiophenone 97% (Irgacure 1173), donkey anti-rabbit IgG (H + L), Alexa Fluor® 488 conjugate (A-21206, Invitrogen), and buffered oxide etchant (BOE) were supplied by Sigma-Aldrich. Irgacure 1173, a photoinitiator, was used in radiation curing in the polymerization of PEGDA.

2.2. Protocol for IOPC Fabrication. The fabrication of IOPCs was performed following Scheme 1 [22, 23]. Herein, 0.5 mL silica sol suspension was dropped onto a microscope slide after covering with a hydrophobic thin layer and dried in air for 1 day at room temperature. The mixture of 99 wt% PEGDA and 1 wt% 2-hydroxy-2-methylpropiophenone was then added into the dried SiO_2 for 5 minutes and exposed under the UV light (312 nm) for 5 minutes for the polymerization process. Finally, the chip was etched by BOE for few hours to obtain the IOPCs before being washed by pure water several times.

2.3. Instruments. The spectrometer processor (Ocean Optics QE Pro-FL), which has a wavelength range of 350 nm–1100 nm, in conjunction with a halogen light source (Ocean Optics HL-2000) was used to determine the reflected spectra. The fluorescent images of the samples were measured using a fluorescent microscope (BX51, Olympus), whereas the fluorescent intensity was analysed by the ImageJ software. Scanning electron microscopy (SEM, Hitachi S-4800; acceleration of 15–20 kV and working electrode distance of 4–5 mm) was used to characterize the surface morphology. Fourier transform infrared spectroscopy (FTIR, FTIR-PerkinElmer Spectrum 10.5.2) measurements were recorded at the atmospheric pressure with a resolution of 4 cm^{-1} using p-polarized radiation. X-ray diffraction data were collected using Bruker D8 (20 kV, 5 mA) equipped with a LynxEye detector and a conventional Cu anode. Diffractograms were collected at a step of 0.25 s.

3. Results and Discussion

3.1. Characterizations of PEGDA/SiO_2 and IOPCs

3.1.1. FT-IR Spectrum. The interactions between PEGDA and SiO_2 are determined via the FT-IR analysis. Figure 1 shows the FT-IR spectra of SiO_2, PEGDA, and PEGDA/SiO_2. The characteristic peaks belonging to SiO_2 are clearly observed in curve (a). The bending vibration of the Si–O group is recorded at the wavenumber of 478 cm^{-1}, while the peak at 949 cm^{-1} is assigned to the vibration of Si–OH. The peaks at 801 cm^{-1} and 1099 cm^{-1} are related to the vibration of the Si–O–Si group. The vibrations of –OH groups are found at 1634 cm^{-1} and 3423 cm^{-1} [27, 28]. The FT-IR spectrum of PEGDA (curve (b)) shows a typical peak of the carbonyl group (C=O) at the wavelength of 1724 cm^{-1}, whereas the peak at the wavelength of 2921 cm^{-1} is attributed to the CH_2 group of PEGDA [29]. The spectrum of PEGDA/SiO_2 (curve (c)) shows all dominant peaks corresponding to both PEGDA and SiO_2. Noticeably, those are related to the methylene group (CH_2), C=O, and Si-O functional surface groups. These results clearly indicate that PEGDA particles have been successfully grafted to SiO_2 spheres via physical interactions [27, 30].

3.1.2. SEM Images. As seen in Figure 2(a), PEGDA/SiO_2 template comprises many SiO_2 spherical particles with a diameter of 300 nm, which are covered by a PEGDA thin film. After etching, the inverse opal photonic structure is created, which contains a large number of micropores with a diameter of ~270 nm, as seen in Figure 2(b). It is obvious that the diameter of air spherical is shrunk, leading to the variation of the wavelength of the reflected light due to effects on the propagation of electromagnetic waves in a limited frequency range, as discussed below.

3.1.3. XRD Analysis. XRD measurement was performed to study the characteristics of PEGDA/SiO_2 before and after etching with BOE. The obtained XRD results for SiO_2, PEGDA/SiO_2 template, and the IOPCs showed only one

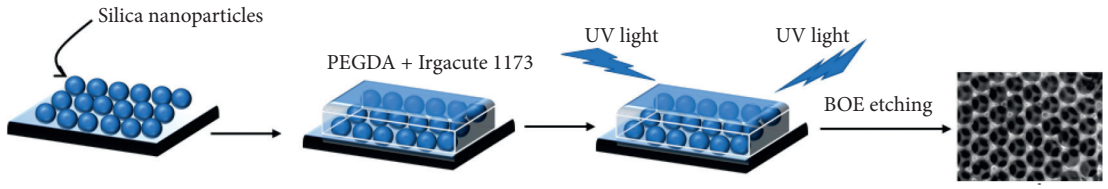

Scheme 1: Protocol for the fabrication of IOPCs.

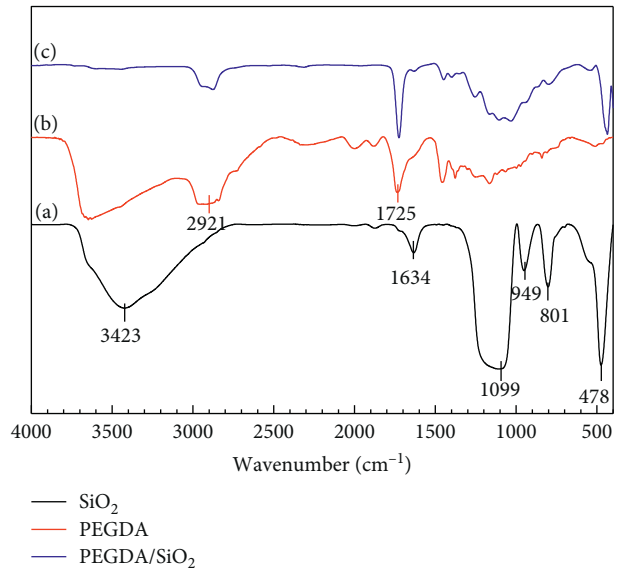

Figure 1: FT-IR spectra of SiO_2 (curve (a)), PEGDA (curve (b)), and PEGDA/SiO_2 (curve (c)).

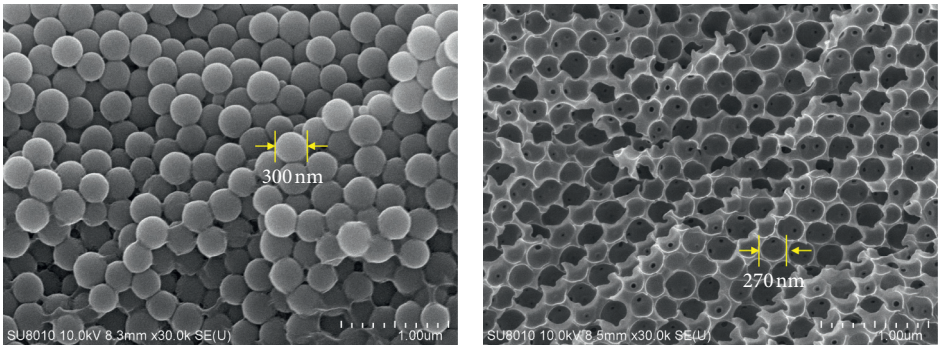

(a) (b)

Figure 2: SEM images of PEGDA/SiO_2 before (a) and after etching with BOE (b).

peak at $2\theta = 22^{\circ}$ (see supplemental information (available here)). The appearance of this peak is a feature of the amorphous state of silica materials [31] and indicates that the fabrication of IOPCs is not influenced by the etching process.

3.2. Reflectance Spectra. The wavelength of reflection peaks (λ) can be estimated based on Bragg's equation as follows [32]:

$$\lambda = 1.633\ d n_{\text{average}}, \tag{1}$$

where d (nm) is the center-to-center distance between two neighbouring mesopores and n_{average} is the average refractive index of the studied materials. According to the product specification sheet, the refractive indexes of SiO_2 particles and PEGDA materials are about 1.378 and 1.463, respectively. The average refractive index of the PEGDA/SiO_2 and IOPCs in the air can be calculated using the following equation [32, 33]:

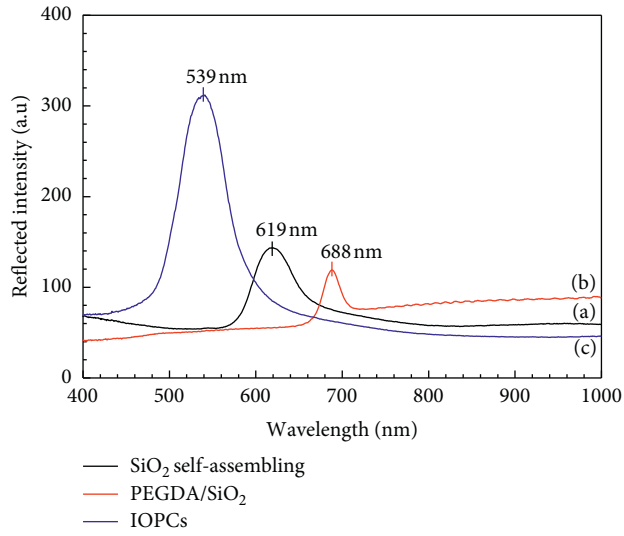

Figure 3: Reflection spectra for SiO_2 self-assembling (curve (a)), PEGDA/SiO_2 (curve (b)), and the IOPCs (curve (c)).

(a) (b) (c)

Figure 4: Photographs of SiO_2 self-assembling (a), PEGDA/SiO_2 (b), and the IOPCs (c).

$$n^2 = (1 - \Phi)n_1^2 + \Phi n_2^2, \quad (2)$$

where n_1 is the refractive index of colloidal crystal, n_2 is the refractive index of the surrounding environment, and Φ is the void ratio of colloidal crystal.

The calculated average refractive indexes of the PEGDA/SiO_2 and the IOPCs were 1.40 and 1.12, respectively. Obviously, the refractive index of the PEGDA/SiO_2 is decreased after etching because of the replacement of SiO_2 spheres in the template by voids. In addition, the wavelengths of reflection peaks of SiO_2, PEGDA/SiO_2, and the IOPCs calculated from equation (1) are 632, 686, and 548, respectively, which are slightly different from the position of reflection peaks at 619, 688, and 539 nm, respectively, as shown in Figure 3.

This difference is due to the decrease in the diameter of micropores as seen in the SEM images. Thus, there is a good agreement between the wavelengths of reflection peaks shown in the reflection spectra and those calculated by Bragg's equation. The reflection spectra shown in Figure 3 exhibit a remarkable stopband blue shift for the IOPCs when the average refractive index decreases and there is a decrease in the diameter of micropores. This can be clearly observed in images shown in Figure 4, in which the observed colour of SiO_2 self-assembling, PEGDA/SiO_2, and the IOPCs is changed from the red colour to orange and green colours correspond to the wavelengths of their photonic stopbands at 688 nm, 619 nm, and 539 nm, respectively. These colour changes exhibit how PhCs made of different materials modify the propagation of light through the photonic stopband. These obtained results are similar to those reported by Subramania and coworkers [34], in which the authors have shown a systematic shift of the reflection peak to longer wavelengths with increasing the diameter of spheres.

3.3. Fluorescent Properties. In order to investigate the effects of the IOPCs on the fluorescence enhancement for Fluor® 488 dye, an accurate amount of 1.0 mg/mL this dye was dropped onto the control PEGDA/SiO_2 template and the IOPCs sample. The Fluor® 488 dye, which is a bright and green-fluorescent dye, has an absorption peak at a wavelength of 496 nm and a maximum emission around 519 nm. Figures 5 and 6 compare the fluorescence intensity of Fluor® 488 dye infiltrated onto the PEGDA/SiO_2 template (non-IOPCs) and the IOPCs sample. The experimental data clearly indicate that over 7.7-fold fluorescence enhancement was achieved for Fluor® 488 dye infiltrated onto the IOPCs sample in comparison with onto the control template. The fluorescence enhancement occurs owing to the fact that the

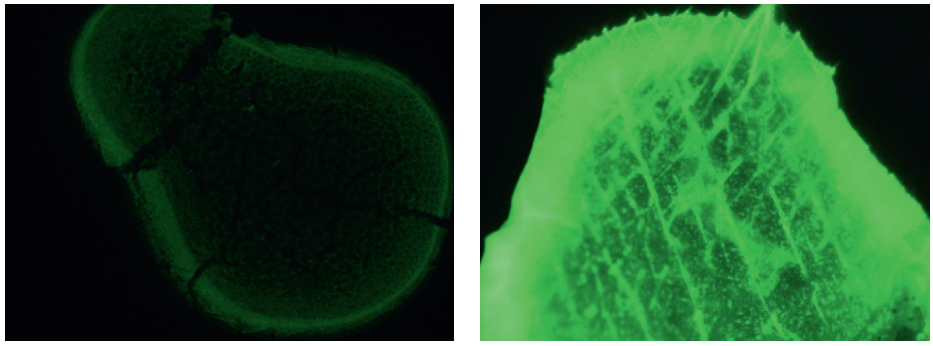

(a) (b)

Figure 5: Fluorescence images of PEGDA/SiO_2 (a) and the IOPCs, for Fluor® 488 dye (b).

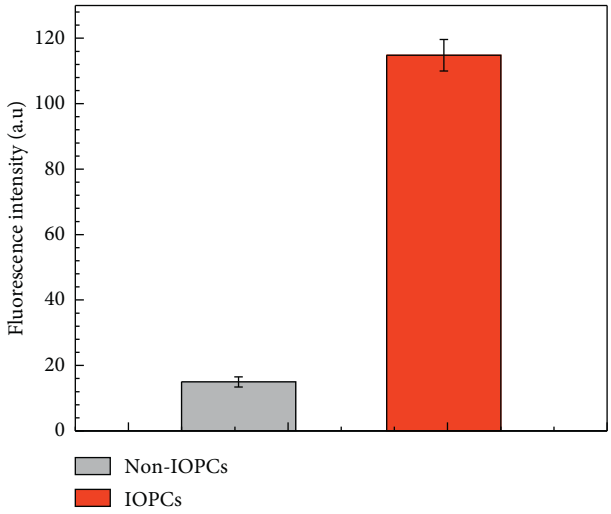

Figure 6: Fluorescence intensities of PEGDA/SiO_2 (non-IOPCs) and the IOPCs for Fluor® 488 dye.

stopband of the IOPCs (539 nm) overlaps the emission of fluorescent Fluor® 488 dye (519 nm), leading to a local resonance mode for the propagation of emission.

In the context that many studies have been attempting to improve the fluorescence enhancement of PhCs, such as studies of the introduction of dyes into the PhCs by different methods [35], effects of lattice period, resonant mode polarization, and symmetry on the enhancement effect of PhCs comprised of colloidal quantum dots [36], the resonant interactions between the localized surface plasmon of gold nanoparticles and the emission of the dye infiltrated into the PhCs [37], or the formation of host-guest complexes between Rhodamine B and cucurbituril [38], our obtained results demonstrate for the first time the fluorescence enhancement of Fluor® 488 dye infiltrated onto the IOPCs which is made of PEGDA/SiO_2. In addition, Fluor® 488 dye is one of the Alexa Fluor dyes, which can be conjugated directly to primary antibodies or to secondary antibodies to amplify signal and sensitivity, since we believe the results of this work can be extended to studies in the field of biological system that might benefit from the added sensitivity afforded by this approach.

4. Conclusions

The inverse opal photonic crystals (IOPCs) fabricated by etching the SiO_2 spheres from the template composed of poly(ethylene glycol) diacrylate (PEGDA) and SiO_2 within this thin layer (PEGDA/SiO_2) have been fabricated. This process induced a reduction of air sphere diameter lowering to ~270 nm. This led to a decrease of the average refractive index of the fabricated IOPCs from 1.40 to 1.12. Consequently, a blue shift of the stopband was achieved. In addition, the IOPCs exhibited a significant enhancement for Fluor® 488 dye up to 7.7-fold in comparison with the control PEGDA/SiO_2 template. Such obtained results can be helpful for studies in the field of biological system to improve the sensitivity of sensing.

Data Availability

All the data and supporting materials are included within the article.

Conflicts of Interest

The authors declare that there are no conflicts of interest regarding the publication of this paper.

Acknowledgments

This study was funded by a Grant-in-Aid for the Project no. NCVCC 06.13/20-20 approved by the decision of 2589/QĐ-VHL of Vietnam Academy of Science and Technology.

Supplementary Materials

Supp. 1: XRD patterns of SiO_2 (a), PEGDA/SiO_2 (b), and the IOPCs (c). (*Supplementary Materials*)

References

[1] M. O. A. Erola, A. Philip, T. Ahmed, S. Suvanto, and T. T. Pakkanen, "Fabrication of Au- and Ag-SiO_2 inverse opals having both localized surface plasmon resonance and Bragg diffraction," *Journal of Solid State Chemistry*, vol. 230, pp. 209–217, 2015.

[2] D. P. Josephson, M. Miller, and A. Stein, "Inverse opal SiO_2 photonic crystals as structurally-colored pigments with additive primary colors," *Zeitschrift für anorganische und allgemeine Chemie*, vol. 640, no. 3-4, pp. 655–662, 2014.

[3] G. I. N. Waterhouse and M. R. Waterland, "Opal and inverse opal photonic crystals: fabrication and characterization," *Polyhedron*, vol. 26, no. 2, pp. 356–368, 2007.

[4] R. C. Schroden, M. Al-Daous, C. F. Blanford, and A. Stein, "Optical properties of inverse opal photonic crystals," *Chemistry of Materials*, vol. 14, no. 8, pp. 3305–3315, 2002.

[5] Y. Zhang, L. Mu, R. Zhou et al., "Fluoral-p infiltrated SiO_2 inverse opal photonic crystals as fluorescent film sensors for detecting formaldehyde vapor," *Journal of Materials Chemistry C*, vol. 4, no. 41, pp. 9841–9847, 2016.

[6] S. Tomiyama, R. Takahashi, S. Sato, T. Sodesawa, and S. Yoshida, "Preparation of Ni/SiO_2 catalyst with high thermal stability for CO_2-reforming of CH_4," *Applied Catalysis A: General*, vol. 241, no. 1-2, pp. 349–361, 2003.

[7] D. Radivojević, K. Seshan, and L. Lefferts, "Pt/SiO_2 catalyst preparation: high platinum dispersions by using low-temperature treatments," in *Studies in Surface Science and Catalysis*, E. M. Gaigneaux, M. Devillers, D. E. De Vos et al., Eds., pp. 529–536, Elsevier, Amsterdam, Netherlands, 2006.

[8] F. Xue, W. Chen, X. Song, X. Cheng, and Y. Ding, "Promotional effects of Cr and Fe on Rh/SiO_2 catalyst for the preparation of ethanol from CO hydrogenation," *RSC Advances*, vol. 6, no. 42, pp. 35348–35353, 2016.

[9] O. Sahu and N. Singh, "13—significance of bioadsorption process on textile industry wastewater," in *The Impact and Prospects of Green Chemistry for Textile Technology*, I. Shahid ul and B. S. Butola, Eds., pp. 367–416, Woodhead Publishing, Sawston,UK, 2019.

[10] M. Zhao, X. Yang, T. L. Church, and A. T. Harris, "Novel $CaO\text{-}SiO_2$ sorbent and bifunctional $Ni/Co\text{-}CaO/SiO_2$ complex for selective H_2 synthesis from cellulose," *Environmental Science & Technology*, vol. 46, no. 5, pp. 2976–2983, 2012.

[11] T.-H. Ko, S. Wang, F.-H. Chang, and C.-Y. Chu, "Performance of $ZnMn_2O_4/SiO_2$ sorbent for high temperature H_2S removal from hot coal gas," *RSC Advances*, vol. 7, no. 57, pp. 35795–35804, 2017.

[12] D. A. Loy, "Sol–Gel processing," in *Encyclopedia of Physical Science and Technology*, R. A. Meyers, Ed., pp. 257–276, Academic Press, New York, NY, USA, Third edition, 2003.

[13] S. Ehrling, C. Kutzscher, P. Freund, P. Müller, I. Senkovska, and S. Kaskel, "$MOF@SiO_2$ core-shell composites as stationary phase in high performance liquid chromatography," *Microporous and Mesoporous Materials*, vol. 263, pp. 268–274, 2018.

[14] C. Li, J. Li, H. Tang, X. Yang, Q. Fei, and C. Sun, "A non-enzymatic electrochemical biosensor based on SiO_2-Au nanoparticles for hemoglobin detection," *Analytical Methods*, vol. 9, no. 8, pp. 1265–1272, 2017.

[15] N. Massad-Ivanir, G. Shtenberg, T. Zeidman, and E. Segal, "Construction and characterization of porous SiO_2/hydrogel hybrids as optical biosensors for rapid detection of bacteria," *Advanced Functional Materials*, vol. 20, no. 14, pp. 2269–2277, 2010.

[16] W. Lee, T. Kang, S.-H. Kim, and J. Jeong, "An antibody-immobilized silica inverse opal nanostructure for label-free optical biosensors," *Sensors*, vol. 18, no. 1, p. 307, 2018.

[17] Y. Zhang, Q. Li, P. Guo et al., "Fluorescence-enhancing film sensor for highly effective detection of Bi^{3+} ions based on SiO_2 inverse opal photonic crystals," *Journal of Materials Chemistry C*, vol. 6, no. 27, pp. 7326–7332, 2018.

[18] Y. Zhang, Y. Sun, J. Liu, P. Guo, Z. Cai, and J.-J. Wang, "Polymer-infiltrated SiO_2 inverse opal photonic crystals for colorimetrically selective detection of xylene vapors," *Sensors and Actuators B: Chemical*, vol. 291, pp. 67–73, 2019.

[19] H. Li, J. Wang, Z. Pan et al., "Amplifying fluorescence sensing based on inverse opal photonic crystal toward trace TNT detection," *Journal of Materials Chemistry*, vol. 21, no. 6, pp. 1730–1735, 2011.

[20] Z. Stillman, B. M. Jarai, N. Raman, P. Patel, and C. A. Fromen, "Degradation profiles of poly (ethylene glycol) diacrylate (PEGDA)-based hydrogel nanoparticles," *Polymer Chemistry*, vol. 11, no. 2, pp. 568–580, 2020.

[21] A. Cavallo, M. Madaghiele, U. Masullo, M. G. Lionetto, and A. Sannino, "Photo-crosslinked poly (ethylene glycol) diacrylate (PEGDA) hydrogels from low molecular weight prepolymer: swelling and permeation studies," *Journal of Applied Polymer Science*, vol. 134, pp. 443801–443809, 2017.

[22] J. H. Kim, J. H. Moon, S.-Y. Lee, and J. Park, "Biologically inspired humidity sensor based on three-dimensional photonic crystals," *Applied Physics Letters*, vol. 97, no. 10, p. 103701, 2010.

[23] E. Choi, Y. Choi, Y. H. P. Nejad, K. Shin, and J. Park, "Label-free specific detection of immunoglobulin G antibody using nanoporous hydrogel photonic crystals," *Sensors and Actuators B: Chemical*, vol. 180, pp. 107–113, 2013.

[24] K.-M. Huang, C.-L. Ho, H.-J. Chang, and M.-C. Wu, "Fabrication of inverted zinc oxide photonic crystal using sol-gel solution by spin coating method," *Nanoscale Research Letters*, vol. 8, no. 1, p. 306, 2013.

[25] L. T. Varghese, Y. Xuan, B. Niu, L. Fan, P. Bermel, and M. Qi, "Enhanced photon management of thin-film silicon solar cells using inverse opal photonic crystals with 3D photonic bandgaps," *Advanced Optical Materials*, vol. 1, no. 10, pp. 692–698, 2013.

[26] J. Shin, P. V. Braun, and W. Lee, "Fast response photonic crystal pH sensor based on templated photo-polymerized hydrogel inverse opal," *Sensors and Actuators B: Chemical*, vol. 150, no. 1, pp. 183–190, 2010.

[27] T. Qian, J. Li, H. Ma, and J. Yang, "The preparation of a green shape-stabilized composite phase change material of polyethylene glycol/SiO_2 with enhanced thermal performance based on oil shale ash via temperature-assisted sol-gel method," *Solar Energy Materials and Solar Cells*, vol. 132, pp. 29–39, 2015.

[28] Y. Liang, J. Ouyang, H. Wang, W. Wang, P. Chui, and K. Sun, "Synthesis and characterization of core-shell structured $SiO_2@YVO_4:Yb^{3+}$, Er^{3+} microspheres," *Applied Surface Science*, vol. 258, no. 8, pp. 3689–3694, 2012.

[29] F. Askari, M. Zandi, P. Shokrolahi, M. H. Tabatabaei, and E. Hajirasoliha, "Reduction in protein absorption on ophthalmic lenses by PEGDA bulk modification of silicone acrylate-based formulation," *Progress in Biomaterials*, vol. 8, no. 3, pp. 169–183, 2019.

[30] B. Lin and S. Zhou, "Poly (ethylene glycol)-grafted silica nanoparticles for highly hydrophilic acrylic-based polyurethane coatings," *Progress in Organic Coatings*, vol. 106, pp. 145–154, 2017.

[31] G. Zhang, Y. Xu, D. Xu, D. Wang, Y. Xue, and W. Su, "Pressure-induced crystallization of amorphous SiO_2 with silicon-hydroxy group and the quick synthesis of coesite under lower temperature," *High Pressure Research*, vol. 28, no. 4, pp. 641–650, 2008.

[32] B. Zhang, Y. Cheng, H. Wang et al., "Multifunctional inverse opal particles for drug delivery and monitoring," *Nanoscale*, vol. 7, no. 24, pp. 10590–10594, 2015.

[33] B. Yu, H. Cong, Z. Yang et al., "Preparation of humidity-sensitive poly(ethylene glycol) inverse opal micropatterns using colloidal lithography," *Materials*, vol. 10, no. 9, p. 1035, 2017.

[34] G. Subramania, K. Constant, R. Biswas, M. M. Sigalas, and K.-M. Ho, "Inverse face-centered cubic thin film photonic crystals," *Advanced Materials*, vol. 13, no. 6, pp. 443–446, 2001.

[35] E. Eftekhari, I. S. Cole, and Q. Li, "The effect of fluorophore incorporation on fluorescence enhancement in colloidal photonic crystal," *Physical Chemistry Chemical Physics*, vol. 18, pp. 1743–1749, 2015.

[36] N. Ganesh, I. D. Block, P. C. Mathias et al., "Leaky-mode assisted fluorescence extraction: application to fluorescence enhancement biosensors," *Optics Express*, vol. 16, no. 26, pp. 21626–21640, 2008.

[37] D. Rout and R. Vijaya, "Localized surface plasmon-influenced fluorescence decay in dye-doped metallo-dielectric opals," *Journal of Applied Physics*, vol. 119, pp. 023108–023116, 2016.

[38] A. P. Mohamed and S. Pillai, "Photonic bandgap effect and dye-encapsulated cucurbituril-triggered enhanced fluorescence using monolic colloidal photonic crystals," *New Journal of Chemistry*, vol. 43, pp. 16264–16272, 2019.